

http://pubs.acs.org/journal/aelccp

# In-Situ Polymerized Binder: A Three-in-One Design Strategy for All-Integrated SiO<sub>x</sub> Anode with High Mass Loading in Lithium Ion Batteries

Shuxing Wu, Yajun Yang, Canbin Liu, Tiefeng Liu, Yaping Zhang, Bingkai Zhang, Dong Luo, Feng Pan, and Zhan Lin\*



Cite This: ACS Energy Lett. 2021, 6, 290-297



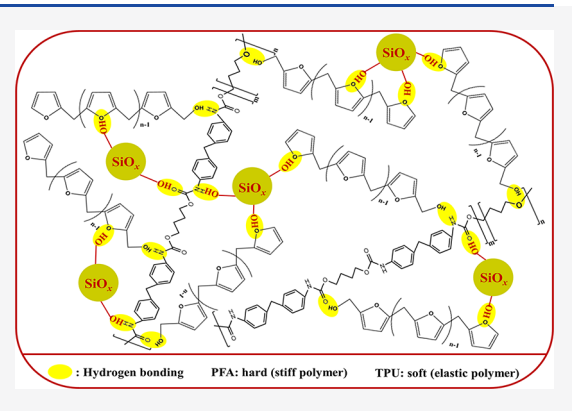
**ACCESS** 

Metrics & More

Article Recommendations

Supporting Information

ABSTRACT: The development of  $SiO_x$  electrode with high mass loading, which is an important prerequisite for practical lithium-ion batteries, remains an arduous challenge by using existing binders. Herein, we propose a three-in-one design strategy for binder systems in all-integrated  $SiO_x$  electrodes. "Hard" poly(furfuryl alcohol) (PFA) and "soft" thermoplastic polyurethane (TPU) are interweaved into 3D conformation to confine  $SiO_x$  particles via in-situ polymerization. In the electrode system, PFA works as a framework and TPU servers as a buffer, and H-bonding interactions are formed between the components. Benefiting from the three-pronged collaborative strategy, PFA-TPU/ $SiO_x$  electrode exhibits an areal capacity of 2.4 mAh cm<sup>-2</sup> at a high mass loading of >3.0 mg cm<sup>-2</sup> after 100 cycles. Such a binder system is also extended to other potential metal oxides anode with high mass loading, or  $SiO_x$  thus shadding light on rational design of functions.



e.g., Fe<sub>2</sub>O<sub>3</sub> and SnO<sub>2</sub>, thus shedding light on rational design of functional polymer binders for high-areal-capacity electrodes.

Tilicon-based materials, e.g., silicon (Si) and silicon suboxide (SiO<sub>x</sub>, 0 < x < 2), are the promising anode candidates for high-energy-density lithium ion batteries (LIBs). Further efforts have manifested that SiO<sub>x</sub> is the prime alternative to Si since SiOx is very effective to accommodate the defects of Si on cycling performance. 1,2 During the first lithiation, the uptake of Li by SiO<sub>x</sub> generates a uniform mixture of Si/Li<sub>2</sub>O/Li silicates (e.g., Li<sub>4</sub>SiO<sub>4</sub> and Li<sub>2</sub>Si<sub>2</sub>O<sub>5</sub>) at nanoscale. The Li<sub>2</sub>O/Li silicates are dispersed uniformly among formed nano-Si, which offers high specific capacity for the SiO<sub>x</sub> anode.<sup>3,4</sup> Meanwhile, the inactive Li<sub>2</sub>O/Li silicates serve as a buffer to effectively alleviate the volume variation of the nano-Si material during cycling and stabilize the interface between anode and electrolyte. 5-7 Due to safety concerns, the volume variation of industrial LIBs is generally limited less than 20% and the corresponding volume change for the anode is better lower than 30%. Nevertheless, non-negligible volume variation ( $\sim$ 200%) impedes practical application of SiO<sub>x</sub> anodes. The construction of robust binders is an admirable method to maintain the structure integrity of Si-based anodes with reduced volume variation during cycling.<sup>8-11</sup> However, it is still vital to develop multipronged design strategies for

binder systems in  $SiO_x$  anodes with high mass loading for practical high-energy-density LIBs.  $^{11-14}$ 

Three auspicious strategies have been widely adopted for binder design. <sup>15</sup> The first one is to construct an interpenetrated 3D network. Binders with interpenetrated 3D structures exhibit strengthening mechanical properties, thus preserving the integrity of the whole electrode. In addition, the 3D network facilitates charge transportation and contributes the formation of a stable SEI layer. The second one is to tune mechanical properties. The elastomer is an interesting polymer type for LIBs since it mitigates the expansion of active materials; however, excessive elasticity allows unrestricted expansion of active materials. The unrestricted expansion results in a prolonged migration path of Li<sup>+</sup> ions and further a decreased rate performance for active materials. <sup>11</sup> In

Received: November 5, 2020 Accepted: December 22, 2020 Published: December 29, 2020

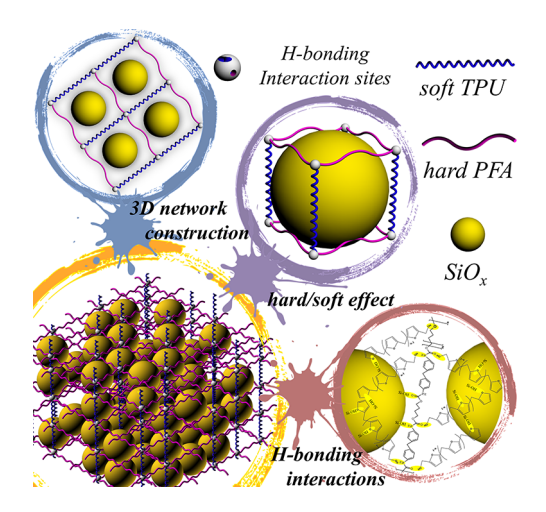




comparison with the elastomer, stiff polymers effectively restrict volume variation and maintain the integrity of electrodes. However, high mechanical stiffness makes the electrode brittle, especially under high mass loading. 16 The integration of the two different types of polymers leads to a great binder system. The elastomer serves as a buffer to tolerate severe volume change of active materials, while stiff polymer constructs a framework to keep electrode integrity. The third one is the creation of H-bonding interactions. Compared with van der Waals force and covalent bond, the hydrogen bond is strong enough while retaining its dynamic nature. 17 The strong interaction and dynamic nature of the hydrogen bond is thought to offer a self-healing effect to rejuvenate broken interactions, dissipate mechanical stress and maintain electrode structure. Importantly, silanol groups (Si-OH) on the SiO<sub>x</sub> surface can be readily used to form a hydrogen bond with polar functional groups, such -OH, -COOR/-COOH, and -NH2. Although each strategy has been well used for Si-based materials, it remains challenging to achieve precise binder systems, i.e., integrating three strategies into one and simultaneously enhancing electrode performance, for Si-based anodes with high mass loading.

Generally, the realization of multipronged strategy requires painstaking procedures, for which a facile route is highly needed. Integrating the fabrication of polymeric binder with the preparation of electrode through an in-situ polymerization route to obtain all-integrated electrodes can simplify electrode preparation process. <sup>18,19</sup> Herein, we introduce a binder system for all-integrated  $SiO_x$  anode with high mass loading by utilizing a three-in-one design strategy. "Hard" poly(furfuryl alcohol) (PFA) and "soft" thermoplastic polyurethane (TPU) chains which possess rich polar functional groups have been integrated into 3D interconnected conformation via in-situ polymerization. The "hard" refers to high stiffness of stiff polymers and the "soft" means high elasticity of elastomer. 8,20,21 Scheme 1 shows the working mechanism of this three-pronged collaborative strategy, i.e., 3D network construction, hard/soft effect, and H-bonding interactions, are simultaneously rolled up. Taking advantage of this binder system, the SiO<sub>x</sub> electrode exhibits a high areal capacity of 2.4

Scheme 1. Schematic Illustration of the Three-in-One Design Strategy for Binder in SiO<sub>x</sub> Anode with High Mass Loading: (1) Constructing Interpenetrated 3D Network, (2) Introducing Hard/Soft Effect to Tune Mechanical Property, and (3) Creating H-Bonding Interactions



mAh cm $^{-2}$  at high mass loading (>3.0 mg cm $^{-2}$ ) after 100 cycles, which is significantly improved in comparison with cases by using carboxyl methylcellulose (CMC), PFA, and TPU. In addition to SiO<sub>x</sub> anodes, the binder system can be generally applicable for other high mass loading oxide anodes including Fe<sub>2</sub>O<sub>3</sub> and SnO<sub>2</sub>.

Hydroxyl methyl group (-CH2-OH) endows FA with facile acid-catalyzed polymerization (Figure S1a). 22,23 Over reaction time, a transparent yellow liquid (FA) becomes a gel (polymerization for 30 min, Video S1) and further form stiff black resin (polymerization for 60 min, Video S2) under the catalysis of oxalic acid. Fourier-transform infrared spectroscopy (FTIR) performed to explore the FA polymerization kinetics (Figure S2). The polymerization results in the decrease in peaks, especially for the - OH stretching band at 3432 cm<sup>-1</sup>, since the -CH2-OH group enables acid-catalyzed polymerization of FA to PFA.<sup>24</sup> Molecular weights of time-dependent PFA were determined by gel permeation chromatography (Table S1). N-methyl-2-pyrrolidone was used as the agent for both FA and TPU, the FA monomers can penetrate into the elastic TPU hydrogel and in-situ polymerize under acid catalysis, thereby, forming an interpenetrated 3D network. When served as binder for commercial SiO, particles (Figure S3), the formed 3D network wraps the SiO<sub>x</sub> particles and prohibits the aggregation of particles, thus forming welldispersed electrodes. Figure S4 shows the thermogravimetric curves of the as-prepared PFA-TPU/SiO<sub>x</sub> electrode. For a further analysis of morphological characteristics of the PFA-TPU/SiO<sub>x</sub> electrode, an easy-to-apply confocal laser scanning microscope (CLSM) was used to image the microstructure (Figure 1). The upper and bottom rows display the 3D images and the intercepted cross-section images, respectively. As displayed in Figure 1, Rhodamine B-tagged PFA excited with 561 nm and flourescein iso-thiocyanate-stained TPU excited with 488 nm present red and green, respectively. Distinct distribution of PFA and TPU in the whole electrode is reflected in the CLSM images. As expected, PFA and TPU interpenetrate each other uniformly and continuously, forming a 3D network to confine the  $SiO_x$  particles (Figure 1c). The 3D interpenetrated network is also demonstrated by the ortho view (Figure S5) and visual video (Video S3) of CLSM.

In the PFA-TPU binder system, hard PFA and soft TPU are interweaved to alter he mechanical properties of the binder system (Video S4). A stress-strain curve for PFA resin in Figure 2a (purple line) shows a typical profile of stiff polymer.<sup>8</sup> The sharp decrease refers to the tearing of the PFA resin when the stress is exceeded. The fracture of PFA resin takes place at the strain of 6.5% after a two-phase increase under the tensile stress of 1.8 MPa. As an elastomer, soft TPU is easily deformable under low tensile stress (Figure 2a, black line and Figure S6). When working as the binder for SiO, anode, the "hard/soft" effect of this polymer binder system was demonstrated by nanoindentation test. Typical load-displacement curves of the electrodes are shown in Figure 2b. At the same indentation depth, the load applied on PFA-TPU/SiO<sub>x</sub> electrode is higher than that of the TPU/SiO<sub>x</sub> electrode and lower than that of the PFA/SiO<sub>x</sub> electrode. The hardness (Figure 2c) and elastic modulus (Figure S7) versus indentation depth of the samples are compared. The  $PFA/SiO_x$  electrode possesses the highest hardness and elastic modulus compared to other electrodes, while the TPU/SiO<sub>x</sub> electrode displays the lowest hardness and modulus. In general, electrodes with a high elastic modulus are quite brittle and tend to fracture

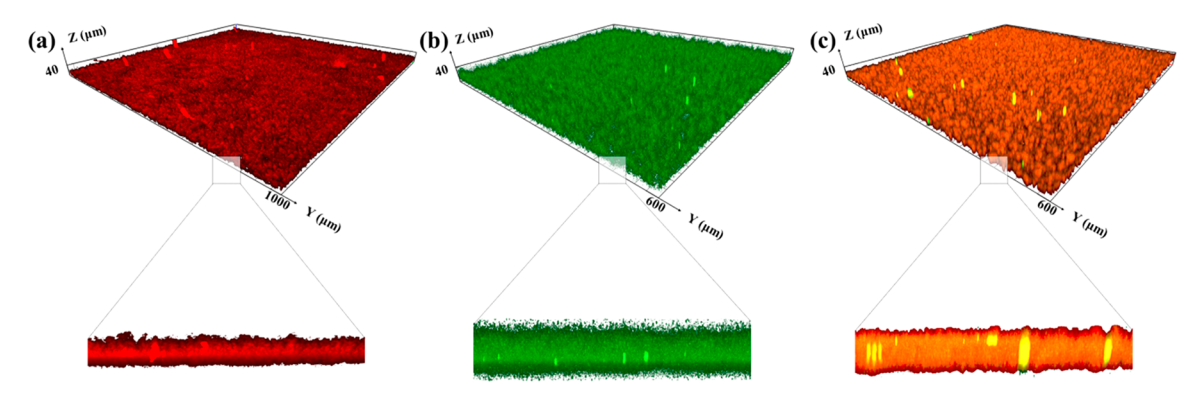


Figure 1. Characterizations of 3D network: CLSM images of PFA-TPU/SiO<sub>x</sub> electrodes with binders of (a) PFA, (b) TPU, and (c) PFA-TPU. The upper row is the 3D images, and the bottom row is the cross-section images (length:  $200 \mu m$ ).

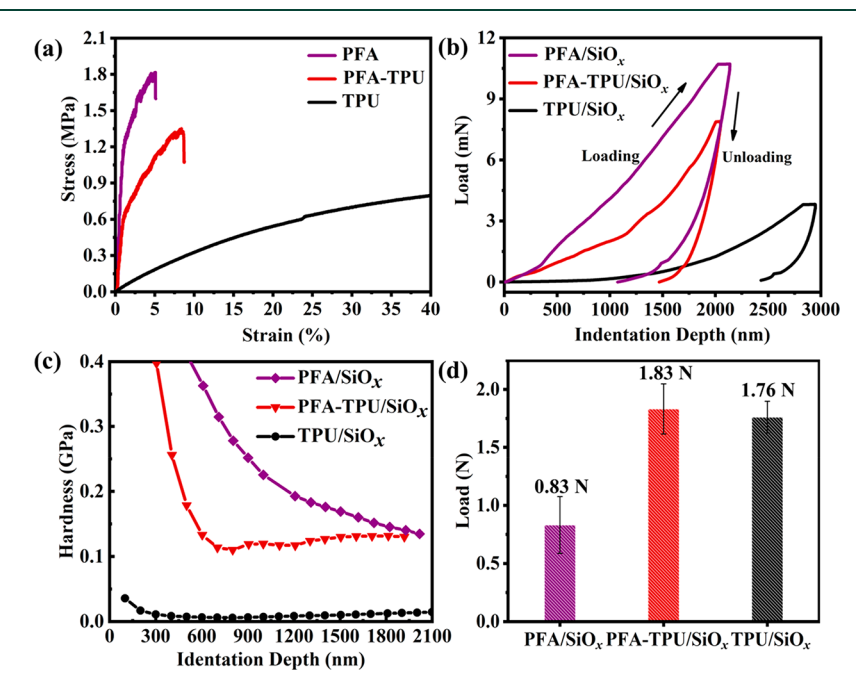


Figure 2. Characterizations of hard/soft effect: (a) strain-stress curve of the polymers and (b) load-indentation depth curve, (c) hardness, and (d) peeling test results of the electrodes.

under high stress, while a low elastic modulus represents an easy deformation under low stress.  $^{25,26}$  After integrating soft TPU into hard PFA, SiO<sub>x</sub> electrodes with the composite binder exhibit mediocre hardness and modulus, suggesting a trade-off between hard PFA and soft TPU. To investigate adhesive strength of binders, conventional 180° peeling tests were carried out (Figure 2d and Figure S8). TPU-based electrodes exhibit higher adhesion strength (1.76 N) than that of PFA based electrode (0.83 N). This observation is ascribed to the fact that PFA possess higher modulus than that of TPU. The adhesion strength of a material is inversely proportional to its modulus.  $^{27}$  PFA-TPU/SiO<sub>x</sub> electrode shows the highest peeling force (1.83 N) and no big fluctuation in the peeling curve, indicating strong adhesion with SiO<sub>x</sub> active material, super P and the copper base.  $^{28}$ 

When PFA incorporates with TPU, H-bonding interactions can be formed between them. Fourier-transform infrared spectroscopy (FTIR) supports the formation of hydrogen bonds between PFA and TPU (Figure 3a). Regarding the combination, the FTIR spectrum of PFA-TPU exhibits the characteristic peaks of PFA and TPU. Specially, the analysis of

the FTIR spectrum shows a massive shift (12 cm<sup>-1</sup>) of the N-H stretching mode of the N-H groups of the TPU (3334 cm<sup>-1</sup>) in comparison to that of the PFA-TPU (3322 cm<sup>-1</sup>), which demonstrates the formation of hydrogen bond between PFA and TPU.<sup>29,30</sup> To understand the interactions between polymer molecular and SiO<sub>x</sub>, we optimized the adsorption configuration by density functional theory (DFT) calculation (Figure 3b-d). The upper part shows the isolated molecular structure. Herein, TPU has been divided into two parts: TPUm and TPU-n segments. There are a large number of H atoms surrounding these molecules when O atoms are on the surface of amorphous SiOx, suggesting potential hydrogen bonding interactions among them. We found that the H atoms interact with the O atoms of amorphous SiO<sub>x</sub> with negative adsorption energies of -1.12 eV (PFA), -0.93 eV (TPU-m), and -0.23eV (TPU-n), respectively, demonstrating the spontaneous Hbonding interactions between PFA-TPU binder and SiO<sub>x</sub>.

To explore the effectiveness of the PFA-TPU binder on high-mass-loading  $SiO_x$  anodes, electrochemical properties of  $SiO_x$  electrodes with the PFA-TPU binder were investigated by assembling Li half-cells. Prior to testing as an anode binder, the

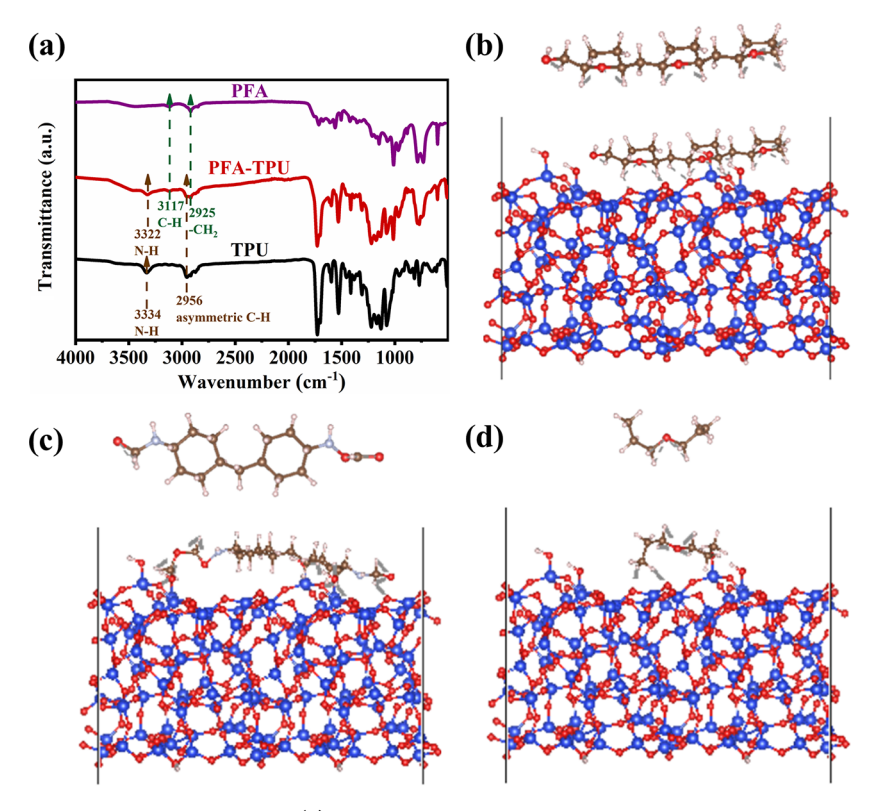


Figure 3. Characterizations of H-bonding interactions: (a) FIIR spectra of PFA, PFA-TPU, and TPU. Adsorption configuration for (b) PFA, (c) TPU-m, and (d) TPU-n over the amorphous SiO $_x$  surface. White, brown, red, dark blue, and light blue spheres represent H, C, O, Si, and N atoms, respectively.

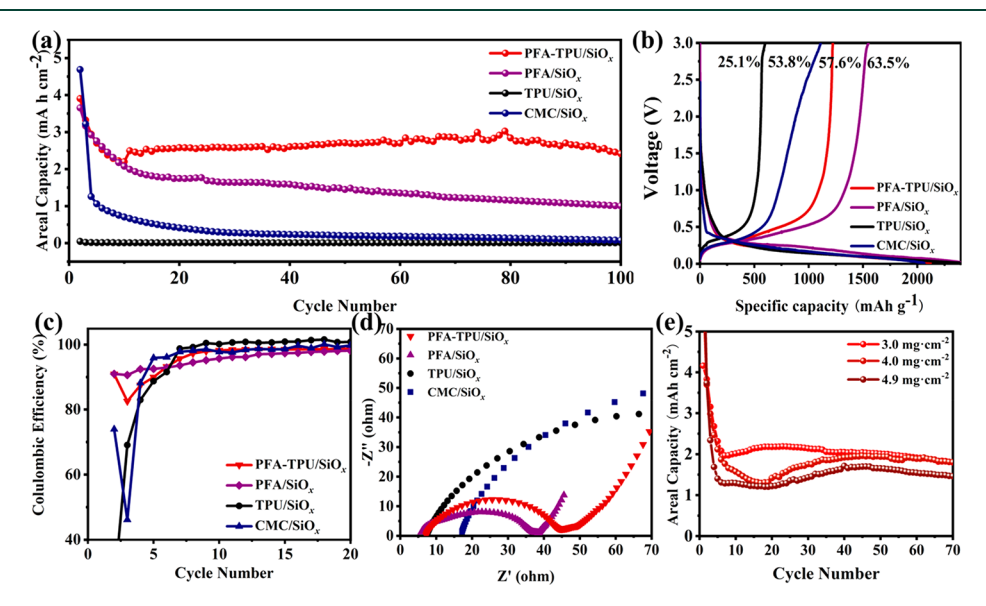


Figure 4. Electrochemical performance of  $SiO_x$  electrode with PFA-TPU binders under high mass loading (>3.0 mg cm<sup>-2</sup>). (a) Cycling performance at 100 mA g<sup>-1</sup>. (b) First charge—discharge curves. (c) Coulombic efficiencies from 2 to 20 cycles. (d) EIS measurements. (e) Cycling performance of the PFA-TPU/SiO<sub>x</sub> electrode at different mass loadings at 100 mA g<sup>-1</sup>.

electrochemical stability of PFA-TPU was evaluated by CV (Figure S9). The CV scan of PFA-TPU discloses that this binder is electrochemically stable, which is indicated by the featureless profile without noticeable oxidation/reduction peaks. Figure 4a presents the cycling performances of  $SiO_x$  electrodes with different binders. The PFA-TPU/ $SiO_x$  electrode shows the best cycling performance compared with the electrodes using CMC, TPU, and PFA binders, and it maintains an areal capacity of 2.4 mAh cm<sup>-2</sup> after 100 cycles.

The optimized ratio of hard PFA and soft TPU is 3:1 (Figure S10). The superior cycling performance of the PFA-TPU/SiO $_x$  electrodes are related to the 3D binder network interacting with the SiO $_x$  active materials and improved mechanical properties tuned by hard/soft polymer systems. This stable performance is also confirmed by CV curves of the PFA-TPU/SiO $_x$  electrode (Figure S11). Figure 4b displays the first discharging/charging profiles of SiO $_x$  with various binders. The first discharging/charging capacities of the PFA-TPU/SiO $_x$ 

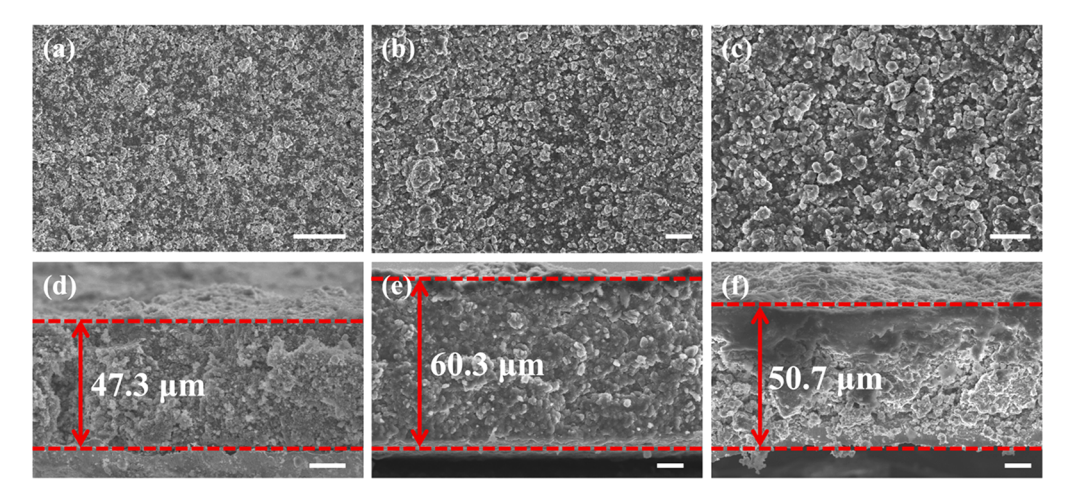


Figure 5. Electrode morphology change. Top-view SEM images of PFA-TPU/SiO<sub>x</sub> electrode (a) before cycle and (b and c) after 50 cycles at various magnification. Cross-section SEM images of PFA-TPU/SiO<sub>x</sub> electrode (d) before cycling, (e) after 1st lithiation, and (f) after 1st delithiation. The scale bar is 10  $\mu$ m.

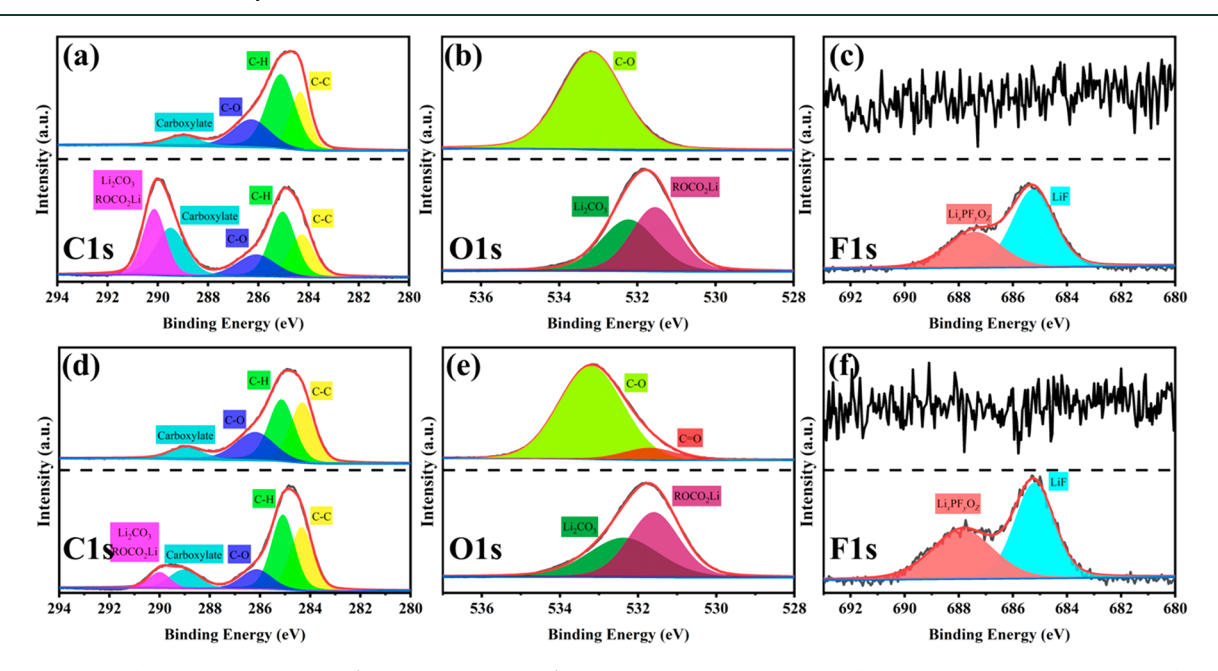


Figure 6. Stability of the SEI layers in PFA/SiO<sub>x</sub> and PFA-TPU/SiO<sub>x</sub> electrodes. XPS spectra of C, O, and F 1s peaks on the surface of SiO<sub>x</sub> anode with (a)–(c) PFA and (d)–(f) PFA-TPU binders before cycle and after 30 cycles. The top and bottom traces in each panel correspond to the SiO<sub>x</sub> anode before and after 30 cycles, respectively.

electrode are 2120.7/1222.2 mAh g-1, indicating an initial Coulombic efficiency (ICE) of 57.6%. The ICE of PFA-TPU/ SiO<sub>x</sub> electrode is higher than those of the CMC/SiO<sub>x</sub> (53.8%) and TPU/SiO<sub>x</sub> electrodes (25.1%). Although ICE of the PFA-TPU/SiO<sub>x</sub> electrode is relatively lower than that of the PFA/ SiO<sub>x</sub> electrode (63.5%) for the first cycle, its Coulombic efficiency increased rapidly and reached a higher Coulombic efficiency than that of the PFA/SiO<sub>x</sub> electrode at the fifth cycle, verifying its superior interface stability in subsequent cycles (Figure 4c). Noting that ICE of PFA-TPU/SiO<sub>x</sub> electrode is not high and low ICE is also the intrinsic shortcoming of SiO<sub>x</sub>based anode materials. High ICE of the PFA-TPU/SiO<sub>x</sub> electrode can be obtained via prelithiation,<sup>31</sup> and the prelithiation is our ongoing work. Here we focus on constructing a binder system for SiO<sub>x</sub> anodes with high mass loading, which has rarely been reported before.

Interfacial properties of the PFA-TPU/SiO<sub>x</sub> electrode were studied by electrochemical impedance spectroscopy (EIS) measurements (Figure 4d and Figure S12). As presented in a Nyquist plot, there are two depressed semicircles in highmedium-frequency region, corresponding to resistances of the solid-electrolyte interphase (R<sub>SEI</sub>) and charge transfer  $(R_{\rm ct})$ . <sup>32,33</sup> PFA-TPU/SiO<sub>x</sub> electrode shows a small semicircle, which is close to that of the PFA/SiO<sub>x</sub> electrode. This trifling increase of the resistances is caused by introducing the TPU polymer since the TPU leads to a high resistance (Figure S12, black line). Here, it should be mentioned that the PFA-TPU/ SiO<sub>x</sub> electrode shows a slightly inferior performance on ICE and EIS tests in comparison to those of the PFA/SiO<sub>x</sub> electrode, but the PFA-TPU/SiO<sub>x</sub> electrodes still present substantially superior cycling performance, which prove the effectiveness of our binder design strategy for the SiO<sub>x</sub> electrodes. Areal capacities of PFA-TPU/SiO<sub>x</sub> electrodes

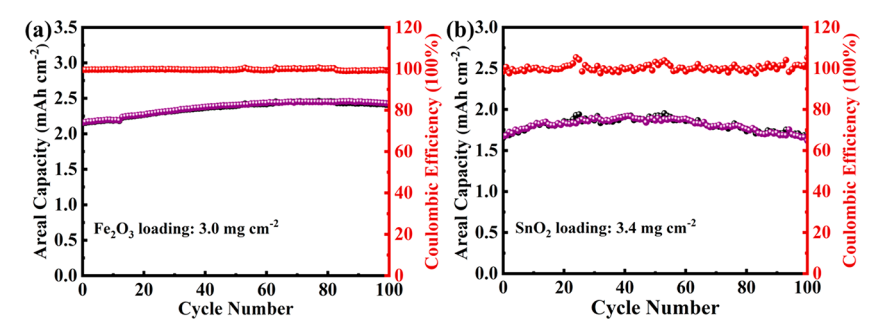


Figure 7. Electrochemical performances of metal oxide anodes with high mass loading after activation treatment. (a) Cycle retention of the PFA-TPU/Fe<sub>2</sub>O<sub>3</sub> electrode with Fe<sub>2</sub>O<sub>3</sub> loading of 3.0 mg cm<sup>-2</sup> at 200 mA g<sup>-1</sup>. (b) Cycle retention of the PFA-TPU/SnO<sub>2</sub> electrode with SnO<sub>2</sub> loading of 3.4 mg cm<sup>-2</sup> at 100 mA g<sup>-1</sup>.

with various active materials mass loadings are disclosed in Figure 4e. The PFA-TPU/SiO<sub>x</sub> electrodes retain decent areal capacity about 1.5 mA h cm<sup>-2</sup> under the mass loading of 4.9 mg cm<sup>-2</sup> after 70 cycles.

To further comprehend remarkably enhanced electrochemical performance of SiO<sub>x</sub> anodes using the PFA-TPU binder, the morphology and structure of the PFA-TPU/SiO<sub>x</sub> electrode before and after cycling were studied. As illustrated in Figure 5a-c, the surface morphology of the PFA-TPU/SiO<sub>x</sub> electrode before and after cycling is similar. No apparent cracks or pulverized particles on the electrodes are observed, suggesting that the PFA-TPU binder has satisfied mechanical capability to accommodate the stress induced by volume changes in SiO<sub>x</sub> particles during lithiation-delithiation. Panels d-f of Figure 5 show cross-section scanning electron microscopy (SEM) images of PFA-TPU/SiO<sub>x</sub> electrode before cycling, at the end of first lithiation, and at the end of first delithiation, respectively. The thickness of the fully lithiated electrode after first discharge expands to 60.3 µm from its origin state (47.3  $\mu$ m), which shows a ~27.5% volume change. Upon charging, the thickness of the lithiated electrode decreases to 50.7  $\mu$ m, presenting a volume variation of 7.2%. Transmission electron microscopy (TEM) images also confirm the robust mechanical capability of the binder system, in which SiO<sub>x</sub> particles are confined in the binder matrix without losing contact both before and after cycling (Figure S13).

Ideal binder should contribute to construct a stable solidelectrolyte interphase (SEI) on the surface of the SiO<sub>x</sub> anode materials. Electrode surfaces are wrapped with binders at the pristine state, while covered with SEI layers after cycling. X-ray photoelectron spectroscopy (XPS) was carried out to understand the effect of binders on the formation of the SEI layer. Obviously, Li 1s and F 1s peaks, which originate from the formed SEI layer, are observed for the cycled electrodes in the XPS survey scan (Figures S14). Figure 6 shows the highresolution spectra of the C 1s, O 1s, and F 1s. Characteristic peaks of C-C (284.3 eV), C-H (285.1 eV), C-O (286.2 eV), and carboxylate (289 eV) are observed (Figure 6a,d).<sup>34</sup> Importantly, an additional peak at 290.1 eV occurs in the cycled electrodes, which is attributed to the formed SEI layer components such as semicarbonate (ROCO2Li) and carbonate (Li<sub>2</sub>CO<sub>3</sub>).<sup>35</sup> Comparison of C 1s spectra of cycled PFA-TPU/ SiO<sub>x</sub> electrodes with that of cycled PFA/SiO<sub>x</sub> electrodes shows that the intensity of the peak corresponding to the SEI layer components is reduced in the cycled PFA-TPU/SiO<sub>x</sub> electrodes. This proves that the cycled PFA-TPU/SiO<sub>x</sub> electrode has a thinner SEI layer, which is because the PFA-TPU binder is well coated onto SiO<sub>x</sub> particles surface and consequently,

parasitic reactions at the SiO<sub>x</sub>/electrolyte interface are inhibited. This result is also verified by O 1s spectra (Figure 6b,e). In O 1s spectra of initial electrodes, PFA/SiO<sub>x</sub> electrodes exhibit only one peak evolution at 533.4 eV, which is assigned to the C—O bond just because PFA simply provides C—O bonds. In addition to the C—O bond, the C= O bond at 531.8 eV, which originates from TPU, appears in the PFA-TPU/SiO<sub>x</sub> electrodes. The C=O bond is weak because the content of TPU in the binder system is low. After 30 cycles, the spectra of both electrodes show a significant difference due to the formation of SEI layer. Typical SEI species of ROCO<sub>2</sub>Li (531.6 eV) and Li<sub>2</sub>CO<sub>3</sub> (532.4 eV) are detected. The relative ratio of the Li<sub>2</sub>CO<sub>3</sub> peak intensity in the cycled PFA-TPU/SiOx electrode is smaller than that of the cycled PFA/SiO<sub>x</sub> electrode, which is consistent with the observation from C 1s above. For F 1s spectra, there are no Fcontaining species in both the initial PFA-TPU/SiO<sub>x</sub> electrode and the PFA/SiO<sub>x</sub> electrode (Figure 6c,f). After 30 cycles, the electrodes contain a peak at 685.2 eV from LiF and a peak at 687.5 eV from Li<sub>x</sub>PF<sub>v</sub>O<sub>z</sub>. Importantly, the LiF peak intensity is strong for the cycled PFA-TPU/SiO<sub>x</sub> electrode. LiF, as an effective passivation layer, is known to have a low Li ion diffusion barrier. Thus, the higher-LiF-containing SEI layers in the PFA-TPU/SiO<sub>x</sub> electrode could be more ionically conductive and allow a stabilized electrode.

In order to reveal the universality of this binder system in enhancing electrochemical performance of metal oxide anode materials, commercial Fe<sub>2</sub>O<sub>3</sub> (Figure S15) and SnO<sub>2</sub> (Figure S16) powders, which have high specific capacities and large volume expansions, are examined following the same test parameters with  $SiO_x$ . Figure 7a shows the cycling performance of the PFA-TPU/Fe<sub>2</sub>O<sub>3</sub> electrode with a high mass loading (3.0 mg cm<sup>-2</sup>) after activation treatment. It exhibits stable cycling for 100 cycles with a steady CE per cycle. The areal capacity of the PFA-TPU/Fe<sub>2</sub>O<sub>3</sub> anode achieves 2.4 mAh cm<sup>-2</sup> after 100 cycles. In addition, this PFA-TPU composite binder system also effectively stabilizes the electrochemical cycling of SnO<sub>2</sub> anodes. As displayed in Figure 7b, the PFA-TPU/SnO<sub>2</sub> electrode with a SnO<sub>2</sub> mass loading of 3.4 mg cm<sup>-2</sup> can charge and discharge well and delivers a high areal capacity of 1.7 mAh cm<sup>-2</sup> after 100 cycles. In this study, active materials loadings of the metal oxide anodes are ultrahigh. The capacities of metal oxides anodes are more susceptible to fade with their mass loading increases since reduced Li-ion diffusion and more complicated reactions occurred on the electrodes. Encouragingly, high areal capacity is maintained under high mass loading by using our binder, suggesting potential application of our PFA-TPU binder in LIBs.

In conclusion, this work uncovers an efficient strategy with regard to advanced binder design for SiO<sub>x</sub> anode with high mass loading. With the use of the designed PFA-TPU binder, the SiO<sub>x</sub> electrode shows a strong capability to preserve the electrode stability; thus, a high areal capacity of 2.4 mAh cm<sup>-2</sup> at a high mass loading is achieved. The following reasons could contribute to this stable electrochemical performance: (1) 3D interpenetrated network formed via in-situ polymerization provides high adhesion to build a robust electrode; (2) two chains interlinked by a hydrogen bond are synergistic to accommodate the volume change of SiO<sub>x</sub>, in which hard PFA acts as the skeleton and soft TPU serves as the filler; (3) strong interaction and dynamical stretchability of hydrogen bonding between PFA-TPU and SiO, exhibit a self-healing effect to restore broken interactions and buffer mechanical stress. Such a binder system is also effective for other metal oxide anodes with high mass loadings, e.g., Fe2O3 and SnO2. This work offers a promising strategy to design effective binders for anodes with a high mass loading and opens up new avenues for practical realization of metal oxide-based LIBs.

## ASSOCIATED CONTENT

# **Supporting Information**

The Supporting Information is available free of charge at https://pubs.acs.org/doi/10.1021/acsenergylett.0c02342.

Details of experimental procedures; additional structural, mechanical properties, and/or composition characterizations of the binders, active materials, and as-prepared electrodes; additional electrochemical data of the asprepared electrodes; molecular structures, FTIR spetra, XRD spectra, TEM images, TG curves, CLSM ortho images, Strain-stress curve, Elastic modulus, Peel off test results, CV curves, cycling performance, impedance spectra, XPS spectra; table of polymerization results (PDF)

Polymerization for 30 min (Video S1) (MP4) Polymerization for 60 min (Video S2) (MP4) 3D interpenetrated network (Video S3) (AVI) Binder system (Video S4) (MP4)

# AUTHOR INFORMATION

### **Corresponding Author**

Zhan Lin — Guangzhou Key Laboratory of Clean Transportation Energy Chemistry, School of Chemical Engineering and Light Industry, Guangdong University of Technology, Guangzhou 510006, China; oorcid.org/0000-0001-5009-8198; Email: zhanlin@gdut.edu.cn

## **Authors**

Shuxing Wu — Guangzhou Key Laboratory of Clean Transportation Energy Chemistry, School of Chemical Engineering and Light Industry, Guangdong University of Technology, Guangzhou 510006, China

Yajun Yang — Guangzhou Key Laboratory of Clean Transportation Energy Chemistry, School of Chemical Engineering and Light Industry, Guangdong University of Technology, Guangzhou 510006, China

Canbin Liu – Guangzhou Key Laboratory of Clean Transportation Energy Chemistry, School of Chemical Engineering and Light Industry, Guangdong University of Technology, Guangzhou 510006, China

- Tiefeng Liu Guangzhou Key Laboratory of Clean Transportation Energy Chemistry, School of Chemical Engineering and Light Industry, Guangdong University of Technology, Guangzhou 510006, China; College of Materials Science and Engineering, Zhejiang University of Technology, Hangzhou 310014, China
- Yaping Zhang State Key Laboratory of Environment-friendly Energy Materials, School of Materials Science and Engineering, Southwest University of Science and Technology, Mianyang 621010, China
- Bingkai Zhang Guangzhou Key Laboratory of Clean Transportation Energy Chemistry, School of Chemical Engineering and Light Industry, Guangdong University of Technology, Guangzhou S10006, China; School of Advanced Materials, Peking University Shenzhen Graduate School, Shenzhen S18055, China
- Dong Luo Guangzhou Key Laboratory of Clean Transportation Energy Chemistry, School of Chemical Engineering and Light Industry, Guangdong University of Technology, Guangzhou 510006, China; orcid.org/0000-0001-7538-5628

Feng Pan — School of Advanced Materials, Peking University Shenzhen Graduate School, Shenzhen 518055, China; orcid.org/0000-0002-8216-1339

Complete contact information is available at: https://pubs.acs.org/10.1021/acsenergylett.0c02342

### Notes

The authors declare no competing financial interest.

## ACKNOWLEDGMENTS

We are thankful the funding supports of the National Natural Science Foundation of China (Project 51874104), Guandong Basic and Applied Basic Research Foundation (Project 2019A1515110861), and Key Technology and Supporting Platform of Genetic Engineering of Materials under States Key Project of Research and Development Plan of China (Project 2016YFB0700600).

### ■ REFERENCES

- (1) Li, G.; Li, J. Y.; Yue, F. S.; Xu, Q.; Zuo, T. T.; Yin, Y. X.; Guo, Y. G. Reducing the volume deformation of high capacity  $SiO_x/G/C$  anode toward industrial application in high energy density lithium-ion batteries. *Nano Energy* **2019**, *60*, 485–492.
- (2) Chen, T.; Wu, J.; Zhang, Q. L.; Su, X. Recent advancement of  $SiO_x$  based anodes for lithium-ion batteries. *J. Power Sources* **2017**, 363, 126–144.
- (3) Xu, Q.; Sun, J. K.; Yu, Z. L.; Yin, Y. X.; Xin, S.; Yu, S. H.; Guo, Y. G.  $SiO_x$  encapsulated in graphene bubble film: an ultrastable Li-ion battery anode. *Adv. Mater.* **2018**, *30* (25), 1707430.
- (4) Hu, Y. S.; Demir-Cakan, R.; Titirici, M. M.; Müller, J. O.; Schlögl, R.; Antonietti, M.; Maier, J. J. A. C. I. E. Superior storage performance of a Si@SiO<sub>x</sub>/C nanocomposite as anode material for lithium-ion batteries. *Angew. Chem., Int. Ed.* **2008**, 47 (9), 1645–1649.
- (5) Park, E.; Yoo, H.; Lee, J.; Park, M. S.; Kim, Y. J.; Kim, H. Dual-size silicon nanocrystal-embedded  $SiO_x$  nanocomposite as a high-capacity lithium storage material. *ACS Nano* **2015**, *9* (7), 7690–7696.
- (6) David, L.; Bhandavat, R.; Barrera, U.; Singh, G. J. N.c. Silicon oxycarbide glass-graphene composite paper electrode for long-cycle lithium-ion batteries. *Nat. Commun.* **2016**, *7*, 10998.
- (7) Zhao, J.; Lee, H. W.; Sun, J.; Yan, K.; Liu, Y. Y.; Liu, W.; Lu, Z. D.; Lin, D. C.; Zhou, G. M.; Cui, Y. Metallurgically lithiated  $SiO_x$  anode with high capacity and ambient air compatibility. *Proc. Natl. Acad. Sci. U. S. A.* **2016**, *113* (27), 7408–7413.

- (8) Liu, T. F.; Chu, Q. L.; Yan, C.; Zhang, S. Q.; Lin, Z.; Lu, J. Interweaving 3D network binder for high-areal-capacity Si anode through combined hard and soft polymers. *Adv. Energy Mater.* **2019**, 9 (3), 1802645.
- (9) Jin, Y.; Li, S.; Kushima, A.; Zheng, X. Q.; Sun, Y. M.; Xie, J.; Sun, J.; Xue, W. J.; Zhou, G. M.; Wu, J.; Shi, F. F.; Zhang, R. F.; Zhu, Z.; So, K.; Cui, Y.; Li, J. Self-healing SEI enables full-cell cycling of a silicon-majority anode with a coulombic efficiency exceeding 99.9%. *Energy Environ. Sci.* **2017**, *10* (2), 580–592.
- (10) Choi, S.; Kwon, T. W.; Coskun, A.; Choi, J. W. Highly elastic binders integrating polyrotaxanes for silicon microparticle anodes in lithium ion batteries. *Science* **2017**, *357* (6348), 279–283.
- (11) Kang, T. X.; Chen, J. H.; Cui, Y.; Wang, Z.; Xu, H. L.; Ma, Z.; Zuo, X. X.; Xiao, X.; Nan, J. N. Three-dimensional rigidity-reinforced  ${\rm SiO_x}$  anodes with stabilized performance using an aqueous multicomponent binder technology. ACS Appl. Mater. Interfaces 2019, 11 (29), 26038–26046.
- (12) Nadimpalli, S. P. V.; Sethuraman, V. A.; Dalavi, S.; Lucht, B.; Chon, M. J.; Shenoy, V. B.; Guduru, P. R. Quantifying capacity loss due to solid-electrolyte-interphase layer formation on silicon negative electrodes in lithium-ion batteries. *J. Power Sources* **2012**, 215, 145–151.
- (13) He, D. L.; Li, P.; Wang, W.; Wan, Q.; Zhang, J.; Xi, K.; Ma, X. M.; Liu, Z. W.; Zhang, L.; Qu, X. H. Collaborative design of hollow nanocubes, in situ cross-linked binder, and amorphous void@SiO<sub>x</sub>@C as a three-pronged strategy for ultrastable lithium storage. *Small* **2020**, *16* (5), 1905736.
- (14) Cao, P. F.; Yang, G.; Li, B. R.; Zhang, Y. M.; Zhao, S.; Zhang, S.; Erwin, A.; Zhang, Z. C.; Sokolov, A. P.; Nanda, J.; Saito, T. Rational design of a multifunctional binder for high-capacity siliconbased anodes. *ACS Energy Lett.* **2019**, *4* (5), 1171–1180.
- (15) Yang, Y. Y.; Wu, S. X.; Zhang, Y. P.; Liu, C. B.; Wei, X. J.; Luo, D.; Lin, Z. Towards efficient binders for silicon based lithium-ion battery anodes. *Chem. Eng. J.* **2021**, *406*, 126807.
- (16) Liu, J.; Galpaya, D. G. D.; Yan, L. J.; Sun, M. H.; Lin, Z.; Yan, C.; Liang, C. D.; Zhang, S. Q. Exploiting a robust biopolymer network binder for an ultrahigh-areal-capacity Li-S battery. *Energy Environ. Sci.* **2017**, *10* (3), 750–755.
- (17) Qi, Y.; Wang, G.; Li, S.; Liu, T. F.; Qiu, J. X.; Li, H. M. Recent progress of structural designs of silicon for performance-enhanced lithium-ion batteries. *Chem. Eng. J.* **2020**, *397*, 125380.
- (18) Liu, Y. J.; Tai, Z. X.; Zhou, T. F.; Sencadas, V.; Zhang, J.; Zhang, L.; Konstantinov, K.; Guo, Z. P.; Liu, H. K. An all-integrated anode via interlinked chemical bonding between double-shelled-yolk-structured silicon and binder for lithium-ion batteries. *Adv. Mater.* 2017, 29 (44), 1703028.
- (19) Liu, T. F.; Tong, C. J.; Wang, B.; Liu, L. M.; Zhang, S. Q.; Lin, Z.; Wang, D. L.; Lu, J. Trifunctional electrode additive for high active material content and volumetric lithium-ion electrode densities. *Adv. Energy Mater.* **2019**, *9* (10), 1803390.
- (20) Ishida, K.; Nishiyama, Y.; Michimura, Y.; Oya, N.; Yoshie, N. Hard-soft conversion in network polymers: effect of molecular weight of crystallizable prepolymer. *Macromolecules* **2010**, *43* (2), 1011–1015.
- (21) Ono, T.; Fujii, S.; Nobori, T.; Lehn, J. M. Soft-to-hard transformation of the mechanical properties of dynamic covalent polymers through component incorporation. *Chem. Commun.* **2007**, *1*, 46–48.
- (22) Guigo, N.; Mija, A.; Vincent, L.; Sbirrazzuoli, N. Chemorheological analysis and model-free kinetics of acid catalysed furfuryl alcohol polymerization. *Phys. Chem. Chem. Phys.* **2007**, *9* (39), 5359–5366.
- (23) Kim, T.; Assary, R. S.; Marshall, C. L.; Gosztola, D. J.; Curtiss, L. A.; Stair, P. C. Acid-catalyzed furfuryl alcohol polymerization: characterizations of molecular structure and thermodynamic properties. *ChemCatChem* **2011**, 3 (9), 1451–1458.
- (24) Sadler, J. M.; Yeh, I. C.; Toulan, F. R.; McAninch, I. M.; Rinderspacher, B. C.; La Scala, J. J. Kinetics studies and character-

- ization of poly(furfuryl alcohol) for use as bio-based furan novolacs. *J. Appl. Polym. Sci.* **2018**, *135* (34), 46608.
- (25) Li, G. R.; Ling, M.; Ye, Y. F.; Li, Z. P.; Guo, J. H.; Yao, Y. F.; Zhu, J. F.; Lin, Z.; Zhang, S. Q. Acacia senegal-inspired bifunctional binder for longevity of lithium-sulfur batteries. *Adv. Energy Mater.* **2015**, 5 (21), 1500878.
- (26) Ling, M.; Xu, Y. N.; Zhao, H.; Gu, X. X.; Qiu, J. X.; Li, S.; Wu, M. Y.; Song, X. Y.; Yan, C.; Liu, G.; Zhang, S. Q. Dual-functional gum arabic binder for silicon anodes in lithium ion batteries. *Nano Energy* **2015**, *12*, 178–185.
- (27) Lee, S. H.; Lee, J. H.; Nam, D. H.; Cho, M.; Kim, J.; Chanthad, C.; Lee, Y. Epoxidized natural rubber/chitosan network binder for silicon anode in lithium-ion battery. *ACS Appl. Mater. Interfaces* **2018**, *10* (19), 16449–16457.
- (28) Li, J. J.; Zhang, G. Z.; Yang, Y.; Yao, D. H.; Lei, Z. W.; Li, S.; Deng, Y. H.; Wang, C. Y. Glycinamide modified polyacrylic acid as high-performance binder for silicon anodes in lithium-ion batteries. *J. Power Sources* **2018**, *406*, 102–109.
- (29) Rozenberg, M.; Loewenschuss, A.; Marcus, Y. An empirical correlation between stretching vibration redshift and hydrogen bond length. *Phys. Chem. Chem. Phys.* **2000**, 2 (12), 2699–2702.
- (30) Steiner, T. The hydrogen bond in the solid state. *Angew. Chem., Int. Ed.* **2002**, *41* (1), 48–76.
- (31) Liu, Z. H.; Yu, Q.; Zhao, Y. L.; He, R. H.; Xu, M.; Feng, S. H.; Li, S. D.; Zhou, L.; Mai, L. Q. Silicon oxides: a promising family of anode materials for lithium-ion batteries. *Chem. Soc. Rev.* **2019**, 48 (1), 285–309.
- (32) Cao, Z.; Zheng, X. Y.; Huang, W. B.; Wang, Y.; Qu, Q. T.; Zheng, H. H. Dynamic bonded supramolecular binder enables high-performance silicon anodes in lithium-ion batteries. *J. Power Sources* **2020**, 463, 228208.
- (33) Hu, S. M.; Wang, L. D. Y.; Huang, T.; Yu, A. S. A conductive self-healing hydrogel binder for high-performance silicon anodes in lithium-ion batteries. *J. Power Sources* **2020**, 449, 227472.
- (34) Verma, P.; Maire, P.; Novak, P. A review of the features and analyses of the solid electrolyte interphase in Li-ion batteries. *Electrochim. Acta* **2010**, 55 (22), 6332–6341.
- (35) Tang, Y. X.; Deng, J. Y.; Li, W. L.; Malyi, O. I.; Zhang, Y. Y.; Zhou, X. R.; Pan, S. W.; Wei, J. Q.; Cai, Y. R.; Chen, Z.; Chen, X. D. Water-soluble sericin protein enabling stable solid-electrolyte interphase for fast charging high voltage battery electrode. *Adv. Mater.* 2017, 29 (33), 1701828.